Experiments with Lilly's Cloud-Topped Mixed Layer Model

WAYNE H. SCHUBERT

Department of Atmospheric Science, Colorado State University, Fort Collins 80523

(Manuscript received 4 June 1975, in revised form 21 November 1975)

ABSTRACT

Lilly's model of a horizontally homogeneous cloud-topped mixed layer is studied. The model is closed by taking a weighted (weighting factor or entrainment parameter k) average of Lilly's maximum and minimum entrainment cases. The dependence of steady-state solutions on large-scale divergence, sea surface temperature and entrainment parameter k is investigated. By numerical integration the response of the mixed layer to a diurnally varying radiative flux is investigated. Significant variations in the state of the mixed layer and in the convective fluxes are found.

1. Introduction

One of the difficult remaining problems for the modeling of large-scale atmospheric motions is to parametrically include into the heat, moisture and momentum equations the vertical transport and source/sink terms which result from small-scale convective motions. This problem is of particular importance in tropical and subtropical latitudes.

The advent of the meteorological satellite has greatly increased our understanding of the global distribution of convective regimes. For example, Fig. 1, prepared by Miller and Feddes (1971), shows a 4-year average (1967–70) of cloud brightness for January and July.

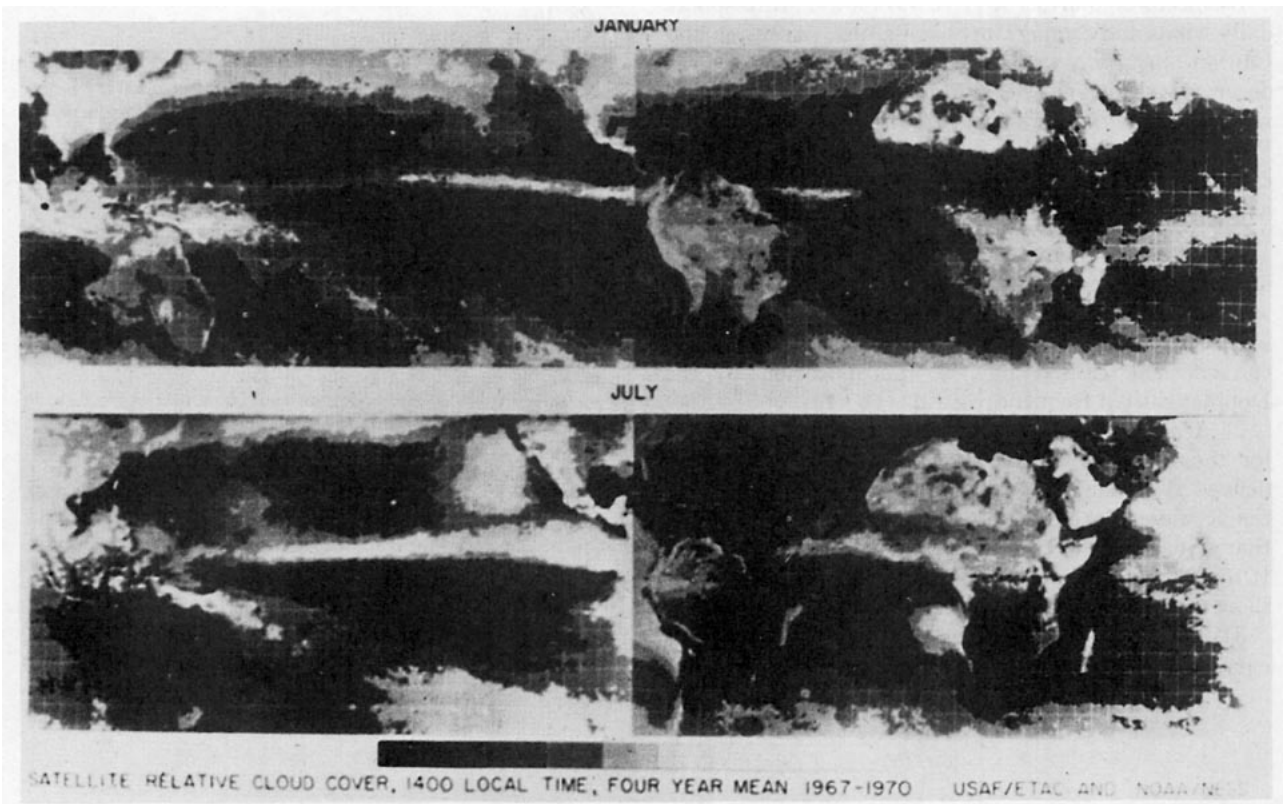

FIG. 1. Four-year average (1967–70) cloud brightness for January and July (from Miller and Feddes, 1971).

One striking feature of Fig. 1 is the bright band of cloudiness between 5° and 10°N associated with the ITCZ. This time-averaged band of cloudiness is the result of westward propagating clusters of deep cumulonimbus clouds and their associated cirrus cloud shields (Chang, 1970). Another striking feature of Fig. 1 is the existence of large areas of low-level stratocumulus convection in the strong subsidence regions to the east of the subtropical highs. A typical instantaneous view of the stratocumulus regime is shown in Fig. 2. It is composed mostly of closed convective cells (Agee and Dowell, 1974) which are generally confined to the lowest kilometer.

A schematic cross section (see also Riehl *et al.*, 1951; Malkus, 1958; Neiburger *et al.*, 1961) from San Francisco to the Hawaiian Islands to the Marshall Islands is shown in Fig. 3. This cross section runs approximately along the trajectories of low-level air parcels. Three regimes are shown. The stratocumulus regime and the trade cumulus regime make up the broad descending branch of the Hadley circulation. The cumulonimbus regime, or ITCZ, makes up the narrow ascending branch of the Hadley circulation.

In the steady-state stratocumulus regime, clouds exist in the face of strong large-scale subsidence through the clouds themselves. Air parcels crossing into the cloud must jump to a higher moisture content and to a lower potential temperature. The jump to higher moisture content is accomplished by a near discontinuity in the upward turbulent flux of total water. The jump to lower potential temperature is accomplished by near discontinuities in the radiative flux and in the turbulent fluxes of liquid water (causing cooling by evaporation) and potential temperature (Lilly, 1968).

In the trade cumulus regime shallow, primarily nonprecipitating cumulus exist in the face of large-scale subsidence. Just below the trade inversion this subsidence, in combination with the large vertical gradients of potential temperature and mixing ratio, causes large warming and drying effects. These effects are opposed

FIG. 2. Typical cloud top view of the convective nature of the stratocumulus regime.

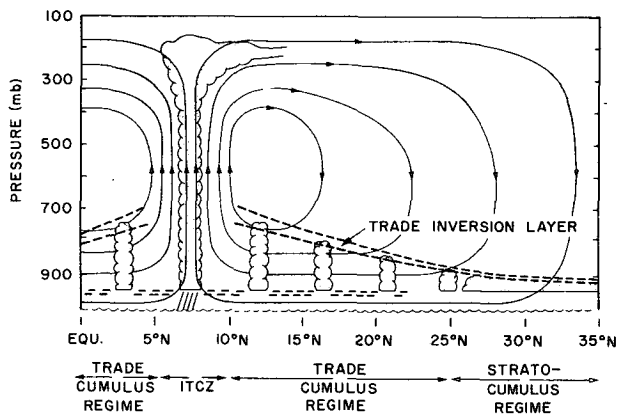

FIG. 3. Schematic cross section from San Francisco to the Hawaiian Islands to the Marshall Islands. Three regimes are shown: the stratocumulus regime and the trade cumulus regime make up the broad descending branch of the Hadley circulation; the cumulonimbus regime, or ITCZ, makes up the narrow ascending branch of the Hadley circulation.

primarily by the cooling and moistening caused by the detrainment of water substance from clouds which lose buoyancy just below the trade inversion. This picture is consistent with the recent BOMEX and ATEX data (Holland and Rasmusson, 1973; Nitta and Esbensen, 1974; Nitta, 1975; Augstein *et al.*, 1973), and with the predictions of Betts (1973).

The tendency of the subtropical atmosphere to divide itself into layers means that air parcels in the downward branch of the Hadley circulation change their potential temperature and moisture content not only gradually when descending through a layer but also in sudden jumps when crossing from one layer to another.

A general circulation model capable of realistic simulation of the Hadley circulation should incorporate the recent advances in cumulus parameterization theory (e.g., Ooyama, 1971; Arakawa and Schubert, 1974) in combination with a unified mixed layer theory, i.e., a mixed layer theory capable of handling both situations where cloud base lies below the top of the mixed layer and situations where cloud base lies above the top of the mixed layer. Such an approach is presently being undertaken for the NCAR GCM by Deardorff (1972, 1976) and for the UCLA GCM by Randall and Arakawa (see Arakawa *et al.*, 1974, and Arakawa, 1974).

As a step in this direction we will study one part of the total problem. In particular, we will study the stratocumulus model developed by Lilly (1968). In Section 2 we review Lilly's model. In Section 3 we investigate its steady-state solutions, and in Section 4 we investigate some of its time-dependent solutions.

2. Review of Lilly's model

In the absence of condensation we can regard the dry static energy $s=c_pT+gz$ and the water vapor mixing

ratio q as conservative quantities. Thus, in a non-saturated mixed layer s and q are constant with height up to the top of the mixed layer p_B, and the lifting condensation level p_C lies above p_B.

When water changes phase we can regard the moist static energy $h=c_pT+gz+Lq$ as a conservative quantity. In addition, if the condensed water is not precipitated but is carried along with the air, we can regard the sum of the water vapor mixing ratio q and the liquid water mixing ratio l as a conservative quantity. Thus, in a saturated non-precipitating mixed layer h and $q+l$ are constant with height up to the top of the mixed layer p_B, and the lifting condensation level p_C lies below p_B. If h and $q+l$ are constant with height in the mixed layer, it follows that the same is true for $s-Ll$. The temperature and moisture fields of the mixed layer are predicted if any two of the three quantities h, $q+l$ and $s-Ll$ are predicted. We have chosen to predict h and $q+l$.

Assuming no variations in the horizontal direction and denoting the mixed layer values of h and $q+l$ by h_M and $(q+l)_M$, the mixed layer budget equations are

$$\frac{\partial h_M}{\partial t}=\frac{g}{p_0-p_B}[(F_h)_0-(F_h)_B], \tag{1}$$

$$\frac{\partial (q+l)_M}{\partial t}=\frac{g}{p_0-p_B}[(F_{q+l})_0-(F_{q+l})_B], \tag{2}$$

where p_0 is the surface pressure and $(F_h)_B$ and $(F_{q+l})_B$ are the turbulent fluxes of h and $q+l$ just below p_B. Above p_B the turbulent fluxes jump to zero. The surface turbulent fluxes of h and $q+l$ are given by

$$(F_h)_0=\rho_0 C_T V_0[h_0^*-h_M], \tag{3}$$

$$(F_{q+l})_0=\rho_0 C_T V_0[q_0^*-(q+l)_M], \tag{4}$$

where ρ_0 is the surface air density, V_0 the surface wind speed, C_T the transfer coefficient, h_0^* the surface saturation static energy, and q_0^* the surface saturation mixing ratio.

Application of the budget equations for h and $q+l$ in the infinitisimally thin layer at the cloud top leads to

$$-\frac{1}{g}\left(\frac{\partial p_B}{\partial t}-\omega_B\right)\Delta h+(F_h)_B=\Delta F_R, \tag{5}$$

$$-\frac{1}{g}\left(\frac{\partial p_B}{\partial t}-\omega_B\right)\Delta (q+l)+(F_{q+l})_B=0, \tag{6}$$

where ω_B is the large-scale vertical p-velocity at p_B, Δh and $\Delta(q+l)$ are the jumps in h and $q+l$ across p_B and ΔF_R is the jump in the radiative flux across p_B. The jump of a function is defined as the value of the function at a pressure slightly lower than p_B minus the value at a pressure slightly higher than p_B; e.g., Δh is defined as $h(p_B^-)-h_M$.

The cloud base pressure p_C is approximately given in terms of the mixed layer total water content $(q+l)_M$ and the saturation mixing ratio of the mixed layer air just above the surface $q^*(p_0^-)$ as

$$\frac{p_0-p_C}{p_0}=\frac{q^*(p_0^-)-(q+l)_M}{b}=\frac{(1+\gamma)[q_0^*-(q+l)_M]-(\gamma/L)[h_0^*-h_M]}{b}, \tag{7}$$

where b is a dimensionless constant and γ is defined in (11).

One additional equation is needed to close the system. Lilly has argued that the turbulent energy balance sets maximum and minimum bounds on the entrainment. The maximum and minimum entrainment conditions proposed by Lilly are respectively

$$\frac{1}{p_0-p_B}\int_{p_B}^{p_0} F_{sv}dp=0 \quad \text{but} \quad F_{sv}\neq 0 \text{ somewhere}, \tag{8}$$

$$(F_{sv})_{\min}=0 \quad \text{but} \quad \frac{1}{p_0-p_B}\int_{p_B}^{p_0} F_{sv}dp>0, \tag{9}$$

where F_{sv} is the flux of virtual dry static energy and is given in terms of the fluxes of moist static energy and total water as

$$F_{sv}=\begin{cases}\beta F_h-\epsilon L F_{q+l}, & p_B<p<p_C\\ F_h-(1-\epsilon\delta)LF_{q+l}, & p_C<p\lesssim p_0.\end{cases} \tag{10}$$

The dimensionless constants appearing in (10) are defined as

$$\left.\begin{aligned}\beta&=\frac{1+\gamma\epsilon(\delta+1)}{1+\gamma}, & \gamma&=\frac{L}{c_p}\left(\frac{\partial q^*}{\partial T}\right)_p\\ \delta&=0.608, & \epsilon&=\frac{c_pT}{L}\end{aligned}\right\}. \tag{11}$$

Since F_{sv} is proportional to the generation of turbulent kinetic energy by buoyancy, the maximum entrainment condition (8) states that regions of positive generation of turbulent kinetic energy are balanced by regions of negative generation, the net generation for the layer thus vanishing. The minimum entrainment condition (9) states that there is no region of negative generation of turbulent kinetic energy and that the net generation for the layer is positive. Thus, all energy dissipation occurs in the positive region. In this paper we shall use a weighted average of (8) and (9), which can be

written[1]

$$\frac{k}{p_0-p_B}\int_{p_B}^{p_0} F_{sv}dp+\tfrac{1}{2}(1-k)(F_{sv})_{\min}=0. \quad (12)$$

Since $0\leqslant k\leqslant 1$, a positive $(F_{sv})_{\min}$ in (12) would require a negative vertically averaged F_{sv}. This is clearly impossible. Thus, the solutions of (12) satisfy

$$\frac{1}{p_0-p_B}\int_{p_B}^{p_0} F_{sv}dp\geqslant 0 \quad \text{and} \quad (F_{sv})_{\min}\leqslant 0. \quad (13)$$

The fluxes of h and $q+l$ are linear in p in the mixed layer, so that

$$F_h=\left(\frac{p-p_B}{p_0-p_B}\right)(F_h)_0+\left(\frac{p_0-p}{p_0-p_B}\right)(F_h)_B, \quad (14)$$

$$F_{q+l}=\left(\frac{p-p_B}{p_0-p_B}\right)(F_{q+l})_0+\left(\frac{p_0-p}{p_0-p_B}\right)(F_{q+l})_B. \quad (15)$$

Using (10), (14) and (15), the entrainment relation (12) can be written

$$\left\{\beta\left[1-\left(\frac{p_0-p_C}{p_0-p_B}\right)^2\right]+\left(\frac{p_0-p_C}{p_0-p_B}\right)^2\right\}(F_h)_B-\left\{\epsilon\left[1-\left(\frac{p_0-p_C}{p_0-p_B}\right)^2\right]+(1-\epsilon\delta)\left(\frac{p_0-p_C}{p_0-p_B}\right)^2\right\}L(F_{q+l})_B$$

$$+\left\{\beta\left(\frac{p_C-p_B}{p_0-p_B}\right)^2+\left[1-\left(\frac{p_C-p_B}{p_0-p_B}\right)^2\right]\right\}(F_h)_0-\left\{\epsilon\left(\frac{p_C-p_B}{p_0-p_B}\right)^2+(1-\epsilon\delta)\left[1-\left(\frac{p_C-p_B}{p_0-p_B}\right)^2\right]\right\}L(F_{q+l})_0$$

$$+\left[\frac{1-k}{k}\right]\min\left\{\begin{array}{c}\beta(F_h)_B-\epsilon L(F_{q+l})_B\\ \beta\left[\left(\frac{p_C-p_B}{p_0-p_B}\right)(F_h)_0+\left(\frac{p_0-p_C}{p_0-p_B}\right)(F_h)_B\right]-\epsilon L\left[\left(\frac{p_C-p_B}{p_0-p_B}\right)(F_{q+l})_0+\left(\frac{p_0-p_C}{p_0-p_B}\right)(F_{q+l})_B\right]\\ \left[\left(\frac{p_C-p_B}{p_0-p_B}\right)(F_h)_0+\left(\frac{p_0-p_C}{p_0-p_B}\right)(F_h)_B\right]-(1-\epsilon\delta)L\left[\left(\frac{p_C-p_B}{p_0-p_B}\right)(F_{q+l})_0+\left(\frac{p_0-p_C}{p_0-p_B}\right)(F_{q+l})_B\right]\\ (F_h)_0-(1-\epsilon\delta)L(F_{q+l})_0\end{array}\right\}=0. \quad (16)$$

Since F_{sv} is linear in pressure in the subcloud layer and in the cloud layer but is discontinuous across cloud base p_C, the minimum F_{sv} may occur at the top of the cloud layer p_B, the bottom of the cloud layer p_C^-, the top of the subcloud layer p_C^+, or the bottom of the subcloud layer p_0. These four possibilities for the minimum F_{sv} are reflected in the four rows within the large braces of (16).

The purpose of introducing the entrainment condition is to close the system by relating the fluxes at some level above the surface to the fluxes at the surface. Once this is done it becomes possible to compute all the fluxes at all the levels. Only then do we know where the minimum F_{sv} occurs. Thus, (16) has a somewhat implicit form. This is of no consequence in steady-state solutions since the steady-state minimum F_{sv} always falls at p_C^+. It is of consequence in time-dependent solutions and is discussed in Section 4.

A special case of (16) occurs when the minimum F_{sv} falls at p_C^+ and $p_C\to p_B$, i.e., the mixed layer becomes non-saturated. Then, using (10), Eq. (16) reduces to $(F_{sv})_B=-k(F_{sv})_0$, which is the customary closure assumption in the non-saturated case.

3. Steady-state solutions

In the steady state the fluxes of h and $q+l$ are constant with height in the mixed layer and are equal to their surface values. Eqs. (1) through (6) can be combined to give

$$h_M=\frac{\dfrac{\omega_B}{g\rho_0C_TV_0}h(p_B^-)+h_0^*-\dfrac{\Delta F_R}{\rho_0C_TV_0}}{\dfrac{\omega_B}{g\rho_0C_TV_0}+1}, \quad (17)$$

$$(q+l)_M=\frac{\dfrac{\omega_B}{g\rho_0C_TV_0}q(p_B^-)+q_0^*}{\dfrac{\omega_B}{g\rho_0C_TV_0}+1}. \quad (18)$$

Cloud base is given by (7). The entrainment relation

[1] The factor $\frac{1}{2}$ in (12) is somewhat arbitrary and is included so that (12) will reduce to the customary closure assumption in the nonsaturated case (see explanation at the end of this section). Omission of this factor simply results in a revised interpretation of the parameter k.

(12) can be written

$$\frac{k}{p_0-p_B}[(F_{sv})_B(p_C-p_B)+(F_{sv})_0(p_0-p_C)] +\tfrac{1}{2}(1-k)(F_{sv})_0=0. \quad (19)$$

The minimum F_{sv} occurs in the subcloud layer because Lilly has shown that in the steady state

$$(F_{sv})_B-(F_{sv})_0=\frac{1-\epsilon(\delta+1)}{1+\gamma}\rho_0 C_T V_0 Lb\frac{p_0-p_C}{p_0}>0. \quad (20)$$

Let us assume that the large-scale subsidence field and the moist static energy and water vapor mixing ratio above the mixed layer are given by

$$\omega_B=D(p_0-p_B), \quad (21)$$

$$h(p_B^-)=h_{00}-\frac{\partial h}{\partial p}(p_0-p_B), \quad (22)$$

$$q(p_B^-)=q_{00}-\frac{\partial q}{\partial p}(p_0-p_B), \quad (23)$$

where h_{00}, $\partial h/\partial p$, q_{00}, $\partial q/\partial p$, and the large-scale divergence D are known constants. We can now compute steady-state solutions using the following numerical values:

$$\rho_0 C_T V_0=0.0129 \text{ kg m}^{-2} \text{ s}^{-1}, \quad \Delta F_R=65.65 \text{ W m}^{-2},$$

$$h_0^*=\begin{cases}310.62 \text{ kJ kg}^{-1}\\ 315.90 \text{ kJ kg}^{-1}\end{cases}$$

$$q_0^*=\begin{cases}9.27\times10^{-3}\\ 10.58\times10^{-3}\end{cases}, \quad h_{00}=313.95 \text{ kJ kg}^{-1},$$

$$\frac{\partial h}{\partial p}=-0.251 \text{ kJ kg}^{-1} \text{ kPa}^{-1}$$

$$q_{00}=3.3\times10^{-3}, \quad \frac{\partial q}{\partial p}=0.043\times10^{-3} \text{ kPa}^{-1},$$

$$p_0=102.0 \text{ kPa}$$

$$D=\begin{cases}3.5\times10^{-6} \text{ s}^{-1}\\ 5.0\times10^{-6} \text{ s}^{-1}\end{cases}, \quad \beta=0.532, \quad \gamma=1.340,$$

$$\epsilon=0.114, \quad b=0.0356.$$

The lower values of h_0^* and q_0^* result from a sea surface temperature of 13°C, the higher values from a temperature of 15°C. Although ΔF_R is not independent of mixed layer variables, for simplicity we shall treat it as so.

The method we have used to compute steady-state solutions is as follows. Choose a value of p_B and compute h_M and $(q+l)_M$ from (17) and (18) using the auxiliary relations (21) through (23). Then compute p_C from (7), F_h and F_{q+l} from (3) and (4), $(F_{sv})_0$ and $(F_{sv})_B$ from (10), and k from (19). This procedure has resulted in an acceptable solution if $0\leqslant k\leqslant 1$ and $p_B\leqslant p_C\leqslant p_0$, and can easily be repeated for many choices of p_B.

The case $h_0^*=310.62$ kJ kg^{-1}, $q_0^*=9.27\times10^{-3}$, $D=5\times10^{-6}$ s^{-1} and $k=0.20$ is shown in Fig. 4. As required by (18), $(q+l)_M$ is a weighted average of $q(p_B^-)$ and q_0^*. As is required by (17), h_M is a weighted average of $h(p_B^-)$ and $h_0^*-\Delta F_R/(\rho_0 C_T V_0)$. For the numerical values given above, $\Delta F_R/(\rho_0 C_T V_0)$ is 5.089 kJ kg^{-1}, and it is the discontinuity in the radiative flux which allows $h_M<h_0^*$ and hence a positive F_h.

When compared from the viewpoint of convective fluxes, the similarities and differences between stratocumulus and trade cumulus are evident. This is illustrated in Fig. 5. Fig. 5a shows vertical profiles of convective fluxes for the steady-state stratocumulus case shown in Fig. 4. LF_{q+l} exceeds F_h, causing F_{s-Ll} to be negative. Fig. 5b shows the observed vertical profiles of the trade cumulus convective fluxes for five undisturbed days during BOMEX. These profiles were computed by Betts (1975) from the heat and moisture budget analysis of Nitta and Esbensen (1974) and the radiation budget analysis of Cox (1973). The profiles are 5-day averages. Instantaneous profiles often show a thinner trade inversion and larger vertical gradients of the fluxes in the trade inversion layer. The trade

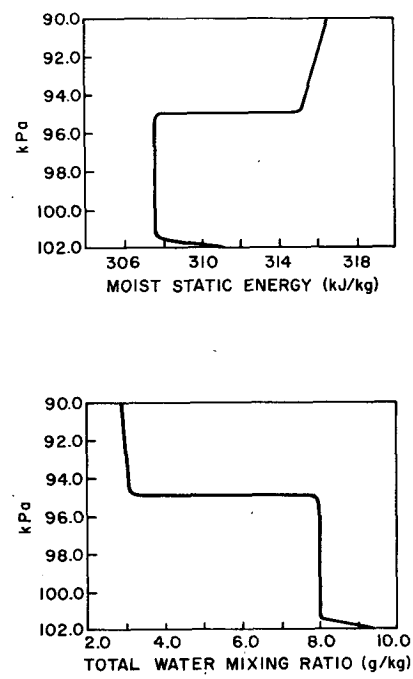

FIG. 4. Steady-state vertical profiles of moist static energy h and total water mixing ratio $(q+l)$ for a large-scale divergence of 5.0×10^{-6} s^{-1}, a sea surface temperature of 13°C, and an entrainment parameter k of 0.20.

cumulus situation has fluxes approximately 3–4 times as strong over a layer 3–4 times as deep as the stratocumulus situation. Except near its top, the trade cumulus subcloud layer has F_{s-Ll} positive, i.e., it has positive surface sensible heat flux and positive Bowen ratio. These subcloud layer differences are consistent with the role of radiation in each regime. In the stratocumulus regime the radiative cooling is confined to a thin layer at cloud top. In the trade cumulus regime radiative cooling extends throughout the cloud layer and subcloud layer, the subcloud layer radiative cooling being balanced by a vertical convergence of the convective flux of $(s-Ll)$.

One major difference between the stratocumulus and trade cumulus regimes is the change of h across cloud top. The air overlying the stratocumulus deck has an h typically 4 kJ kg^{-1} higher than the mixed layer air. The air overlying the inversion above the trade cumulus has an h typically 4 kJ kg^{-1} lower than the cloud layer air. In the trade cumulus regime there is a large convergence of the convective flux of h at cloud top. In the steady state this is used to raise the h of the mean subsiding air to its higher cloud layer value. Although radiation can play a role due to sharp changes in water vapor across the inversion, it is not essential for balance. The situation in the stratocumulus regime is different. The mean subsiding air must jump to a lower value of h, but the convergence of the convective flux of h has just the opposite effect. It is through the discontinuity in radiative flux that it is possible to maintain a steady state with $F_h>0$ and $\Delta h>0$.

The dependence of the steady-state solutions on sea surface temperature, large-scale divergence and entrainment parameter k is shown in Fig. 6. Many of the features of Fig. 6 can be understood from a consideration of the minimum entrainment case. In this case, substitution of (17) and (18) into (19), with the aid of (3), (4), (10) and (21), yields

$$p_0-p_B=\frac{g\Delta F_R}{D\{s_v(p_B^-)-s_{v0}^*\}},$$

where $s_v(p_B^-)$ is the virtual dry static energy just above p_B, and s_{v0}^* is the saturation virtual dry static energy at the ocean surface temperature. This is not an explicit relation for p_B. However, if $[s_v(p_B^-)-s_{v0}^*]$ varies slowly with p_B (the typical case) we can regard it as explicit. Then, for fixed sea surface temperature, the depth of the mixed layer is just proportional to ΔF_R and inversely proportional to D. If ΔF_R is fixed, a decrease in D simply causes the height of the top of the mixed layer to increase until an identical subsidence rate is found. If $h(p_B^-)$ and $q(p_B^-)$ are slowly varying functions of p_B, the same subsidence rate implies the same h_M and $(q+l)_M$ by (17) and (18), the same surface fluxes by (3) and (4), and the same cloud base by (7). All these features are evident in Fig. 6.

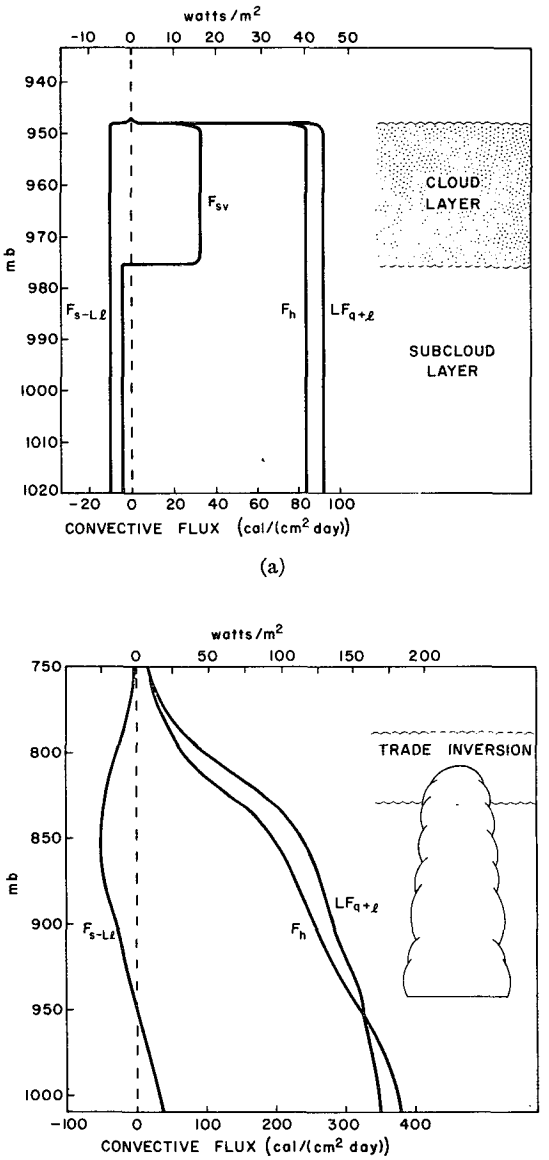

FIG. 5. Steady-state vertical profiles of stratocumulus convective fluxes (a) for the same case as shown in Fig. 4, and observed vertical profiles of trade cumulus convective fluxes (b) for five undisturbed days during BOMEX (after Betts, 1975).

For fixed ΔF_R and fixed D, an increase in sea surface temperature results in increases of p_B, p_C, h_M, $(q+l)_M$, F_h and F_{q+l}. While there is some dependence of the steady-state results on k, this dependence is not large, especially if atmospheric values of k lie between approximately 0.1 and 0.3.

4. Time-dependent solutions

In this section we show some results of numerical integrations of Lilly's model, which consists of Eqs. (1)

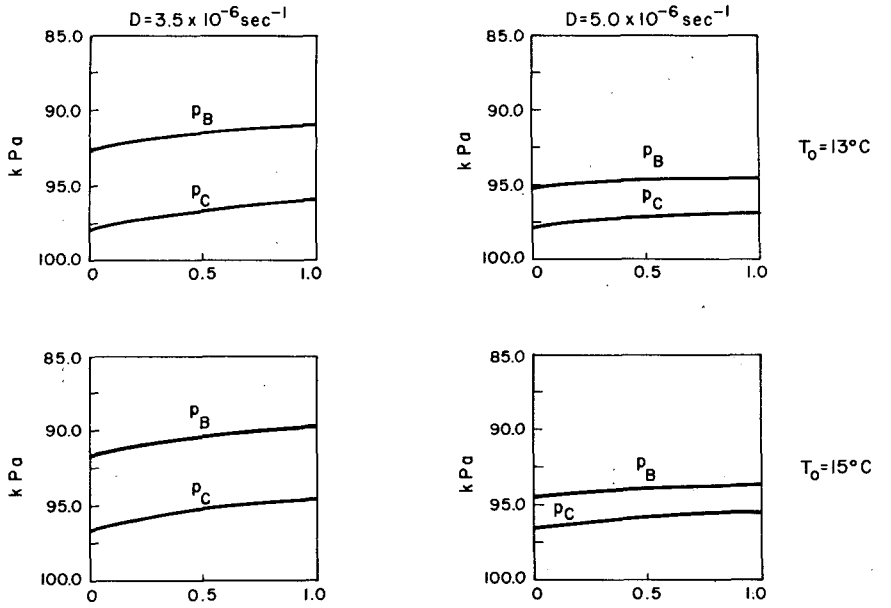

FIG. 6a. p_B and p_c as functions of k. The top two figures are for a sea surface temperature of 13°C, the bottom two for 15°C. The left two figures are for a divergence of 3.5×10^{-6} s^{-1}, the right two for a divergence of 5.0×10^{-6} s^{-1}.

through (7) and (16). As it stands this system is not convenient for numerical integration because (5) and (6) are both prognostic equations for p_B. In order that (5) and (6) predict p_B in a consistent manner it is required that

$$\frac{L\Delta(q+l)}{\Delta h}(F_h)_B - L(F_{q+l})_B = \frac{L\Delta(q+l)}{\Delta h}\Delta F_R. \quad (24)$$

Eq. (5) can be written

$$\frac{\partial p_B}{\partial t} = \omega_B + g\frac{(F_h)_B - \Delta F_R}{\Delta h}. \quad (25)$$

We can now regard our system as composed of the five diagnostic equations [(3), (4), (7), (24) and (16)] and the three prognostic equations [(1), (2) and (25)].

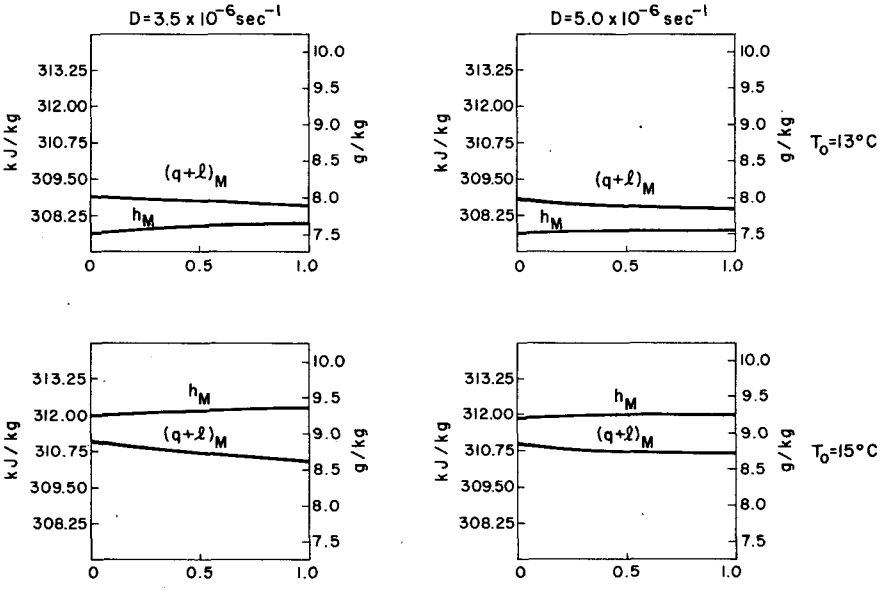

FIG. 6b. As in Fig. 6a except for h_M and $(q+l)_M$.

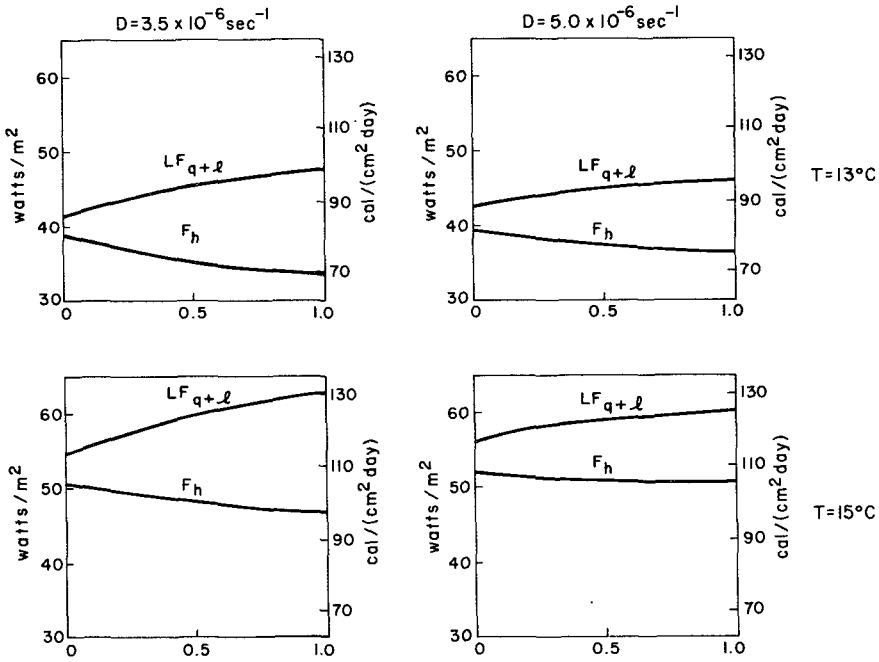

FIG. 6c. As in Fig. 6a except for F_h and LF_{q+l}.

The actual sequence of calculations involved in going from one time step to another is as follows:

(i) Compute the surface fluxes $(F_h)_0$ and $(F_{q+l})_0$ from (3) and (4).
(ii) Compute the cloud base p_C from (7).
(iii) Solve (24) and (16) for $(F_h)_B$ and $L(F_{q+l})_B$.
(iv) Compute the tendencies of h_M and $(q+l)_M$ from (1) and (2), and the tendency of p_B from (25).

This procedure is straightforward except for step (iii). When beginning this step we regard p_B, p_C, Δh, $\Delta(q+l)$, $(F_h)_0$, $L(F_{q+l})_0$ and ΔF_R as known. Then the consistency relation (24) and the entrainment relation (16) are regarded as two equations in the unknowns $(F_h)_B$ and $L(F_{q+l})_B$. These equations take the form

$$\begin{bmatrix} a_{11} & a_{12} \\ a_{21} & a_{22} \end{bmatrix} \begin{bmatrix} (F_h)_B \\ L(F_{q+l})_B \end{bmatrix} = \begin{bmatrix} b_1 \\ b_2 \end{bmatrix}. \tag{26}$$

However, because of the form of (16) the coefficients a_{21} and a_{22} and the constant b_2 are unknown until $(F_h)_B$ and $L(F_{q+l})_B$ are known, i.e., until the location of the minimum F_{sv} is known. Our procedure is to assume that the minimum F_{sv} occurs at p_B, solve (26) for $(F_h)_B$ and $L(F_{q+l})_B$, then using (10), (14) and (15) check to see if the minimum F_{sv} actually occurs at p_B. This procedure is repeated for p_C^-, p_C^+ and p_0. If one and only one of the four possibilities does not lead to a contradiction, we have found the unique solution. It is possible that no solution exists or that more than one solution exists. In the numerical integrations reported here we have not encountered a problem with existence or uniqueness. However, the special case $k=0$ requires extra care. As can be seen from (16), if $k=0$ and the minimum F_{sv} at p_0 case is attempted, both a_{21} and a_{22} vanish, causing the determinant of the coefficients in (26) to vanish. In other words, the minimum entrainment condition applied at p_0 does not close the theory in the time-dependent case.[2] Another interpretation of this difficulty is that there is no guarantee that the minimum entrainment requirement $(F_{sv})_0=0$ will be consistent with (3) and (4).

Perhaps the most interesting time-dependent behavior of the model is that resulting from diurnal variations in radiation. We thus proceed to a brief discussion of the diurnal variation of ΔF_R.

The radiation calculation performed by Lilly is based on considering the cloud to be a blackbody. Lilly estimates that the blackbody assumption is valid if the cloud layer is approximately 125–150 m thick. If this condition holds, the net upward radiant energy flux off the cloud top consists of the upward blackbody flux at the cloud top temperature minus the downward longwave flux from the atmosphere above, minus the solar radiation absorbed by the cloud.

In the time-dependent problem the radiation calculations and mixed layer calculations should be coupled. For example, as p_B, h_M and $(q+l)_M$ change, the cloud top temperature and hence the upward blackbody flux change. In addition, as p_B changes, the downward longwave flux from the atmosphere above changes.

[2] This closure problem does not occur in the steady state. However, in that case a minimum at p_0 can also be interpreted as a minimum at p_C^+.

Rather than make such coupled calculations we have chosen the simple alternative of making ΔF_R a specified function of time, which takes the form

$$\Delta F_R = 90.00 - 69.77 \max\left\{\begin{matrix} 0.202 + 0.779 \cos\left(2\pi \dfrac{t_d}{24}\right) \\ 0 \end{matrix}\right\} \quad [\mathrm{W\ m^{-2}}], \quad (27)$$

where t_d is the time of day measured in hours from local noon. The first term is the net upward longwave flux, while the second term is the solar radiation absorbed by the cloud. At 0500 ($t_d = -7$) and 1900 ($t_d = 7$) the absorbed solar radiation is zero. Such sunrise and sunset hours are found at 33°N in mid-July.

The model was integrated using the classical fourth-order Runge-Kutta scheme with a time step of 10 min. Any reasonable initial condition could be used if several days were allowed for the variables to begin to repeat themselves.

Fig. 7 shows the results of a typical run with a divergence of 5.0×10^{-6} s^{-1}, a sea surface temperature of 13°C, and an entrainment parameter k of 0.20.

The diurnal cycle can be described as follows. $(F_h)_B$ and $L(F_{q+l})_B$ follow very closely the dip in ΔF_R. Just after sunrise $(F_h)_B$ becomes less than $(F_h)_0$ and $L(F_{q+l})_B$ becomes less than $L(F_{q+l})_0$. This means that just after sunrise h_M and $(q+l)_M$ begin to increase. Since the ocean surface temperature is fixed, the increase in h_M and $(q+l)_M$ is accompanied by a decrease in $(F_h)_0$ and $L(F_{q+l})_0$. Just before 1600 $(F_h)_B$ becomes greater than $(F_h)_0$ and $L(F_{q+l})_B$ becomes greater than $L(F_{q+l})_0$. Then h_M and $(q+l)_M$ decrease throughout the evening until just after sunrise the following day. The daytime rise in h_M and $(q+l)_M$ and the daytime fall in $(F_h)_0$ and $L(F_{q+l})_0$ last approximately 10 h, while the corresponding evening and nighttime changes last approximately 14 h. Also shown in Fig. 7a is the variation of $(s-Ll)_M$, which can also be regarded as a measure of the variation of surface air temperature. The surface air temperature falls slightly from morning to afternoon (about 0.14°C), and this tends to slightly lower cloud base. This effect is greatly augmented by the moistening of the layer, the result being that the cloud base is lowered ~130 m. Although the cloud top is also lowered, its variation is not as large, the result being that the cloud layer thickens ~70 m from morning to afternoon. Apparently, the concept of the sun "burning off the stratus" is not valid in the present situation.

We now turn to the question of how well the results of the diurnal computation agree with observation. Neiburger *et al.* (1961) were apparently the first to notice diurnal variations of the stratocumulus over the open ocean. They obtained their observations off the

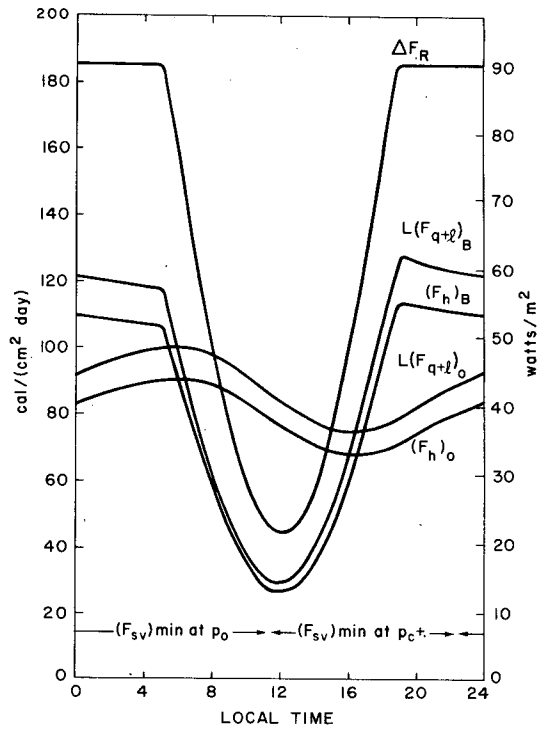

FIG. 7b. Diurnal variation of ΔF_R [see Eq. (27)], $(F_h)_B$, $(F_h)_0$, $L(F_{q+l})_B$ and $L(F_{q+l})_0$.

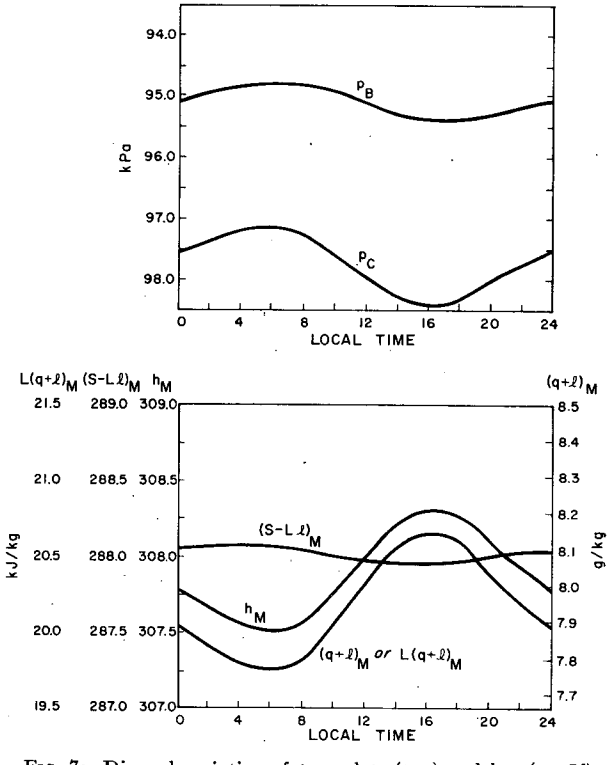

FIG. 7a. Diurnal variation of p_B and p_c (top) and h_M, $(s-Ll)_M$ and $(q+l)_M$ (bottom). Local time 1200 corresponds to noon. The large-scale divergence is 5.0×10^{-6} s^{-1}, the sea surface temperature 13°C, and the entrainment parameter 0.20.

California coast and summarized them as follows:

> "A surprising feature first revealed by the 1949 data is the apparent diurnal variation of inversion height over the entire area, even 500 miles from shore. This was detected by comparing each observation with the average of the ones taken twelve hours before and after. In 52 of the 68 instances in which such a comparison could be made, the morning (local time) inversion heights were higher than the average of adjacent evening ones."

This statement is in agreement with the results shown in Fig. 7.

Kraus (1963) studied the twice daily (0300 and 1500 local time) soundings from weather station N (30°N, 140°W) for five July months from 1958 to 1962. After locating, for each sounding, the pressure level at which the temperature has a minimum (we shall call this level p_B), Kraus computed the second-order difference

$$F = p_B(0300) - \tfrac{1}{2}[p_B(1500 \text{ preceding afternoon}) + p_B(1500 \text{ following afternoon})],$$

for each 0300 sounding. If the mixed layer is deeper at night than during the day, $p_B(0300)$ will be smaller than the average of the two neighboring soundings, and F will be negative. Out of a total of 136 computations of F, Kraus found 40 with $F>0$ and 96 with $F<0$ and thus concluded that the mixed layer at weather station N in July tends to be deeper at night than during the day. The results in Fig. 7 are also in agreement with Kraus' observational study.

5. Conclusions

We have examined both steady-state and time-dependent aspects of Lilly's stratocumulus model. The steady-state results are not highly dependent on the entrainment parameter k and show a deepening and moistening of the layer as divergence is decreased and sea surface temperature is increased. Numerical integration of the model with diurnally varying radiation off cloud top has revealed significant diurnal variations in the state of the mixed layer and in the mixed layer convective fluxes.

It is possible to expand the present study in several directions. The radiation calculation could be coupled to the mixed layer computations. In addition, the atmospheric boundary layer model could be coupled to an oceanic boundary layer model. Another important possibility is to relax the assumption of horizontal homogeneity and to include a $\mathbf{v}\cdot\nabla p_B$ term in (25), a $\mathbf{v}\cdot\nabla h_M$ term in (1) and a $\mathbf{v}\cdot\nabla(q+l)_M$ term in (2). Computations could then be made on a two-dimensional grid of points covering the eastern North Pacific Ocean. For the rapid horizontal variations in sea surface temperature and large-scale divergence typical of coastal California, a rough calculation shows that these horizontal advection terms are probably not negligible.

Lilly's stratocumulus model applies to completely overcast conditions while cumulus parameterization theories generally assume the fractional area of cloudiness is small. It remains a challenging problem to develop a general parameterization theory which can handle stratocumulus, trade cumulus, and the continuous transition from one to the other.

Finally, the time integration of the stratocumulus model has produced diurnal variations for which there is apparently little present observational data. It would seem reasonable to design an observational program with the specific purpose of testing the predictions of the theory. This could perhaps be done with a single well-instrumented aircraft (e.g. Lenschow, 1973).

Acknowledgments. I have benefited greatly from the comments of many colleagues including A. Arakawa, A. K. Betts, S. K. Cox, J. W. Deardorff, W. M. Gray, D. K. Lilly, M. J. Miller and D. Randall. I would also like to thank Mr. James Hack and Ms. Ellen Steiner for their help with the numerical computations. The research reported here has been supported by the GARP Section of the Office of Climate Dynamics, National Science Foundation, Grant DES74-11438.

REFERENCES

Agee, E. M., and K. E. Dowell, 1974: Observational studies of mesoscale cellular convection. *J. Appl. Meteor.*, **13**, 46–53.

Arakawa, A., 1974: Modeling clouds and cloud processes for use in climate models. Presented at JOC International Study Conference on the Physical Basis of Climate and Climate Modeling. Stockholm, July–August, 1974 [Available from the author at the Department of Meteorology, University of California, Los Angeles 90024].

——, A. Mintz and Collaborators, 1974: The UCLA atmospheric general circulation model. Department of Meteorology, UCLA, Los Angeles [Available from the author as shown above].

——, and W. H. Schubert, 1974: Interaction of a cumulus cloud ensemble with the large-scale environment. Part I. *J. Atmos. Sci.*, **31**, 674–701.

Augstein, E., H. Riehl, F. Ostapoff and V. Wagner, 1973: Mass and energy transports in an undisturbed Atlantic trade wind flow. *Mon. Wea. Rev.*, **101**, 101–111.

Betts, A. K., 1973: Nonprecipitating cumulus convection and its parameterization. *Quart. J. Roy. Meteor. Soc.*, **99**, 178–196.

Betts, A. K., 1975: Parametric interpretation of trade-wind cumulus budget studies. *J. Atmos. Sci.*, **32**, 1934–1945.

Chang, C. P., 1970: Westward propagating cloud patterns in the tropical Pacific as seen from time composite satellite photographs. *J. Atmos. Sci.*, **27**, 133–138.

Cox, S. K., 1973: Radiation components of the energy budget for BOMEX. Atmos. Sci. Paper 208, Colorado State University, 43 pp. [Available from NTIS, Springfield, Va., No. COM-73-11950/5AS].

Deardorff, J. W., 1972: Parameterization of the planetary boundary layer for use in general circulation models. *Mon. Wea. Rev.*, **100**, 93–106.

——, 1976: On the entrainment rate of a stratocumulus-topped mixed layer under a strong inversion. Submitted to *Quart. J. Roy. Meteor. Soc.*

Holland, J. Z., and E. M. Rasmusson, 1973: Measurements of the atmospheric mass, energy and momentum budgets over a 500 km square of tropical ocean. *Mon. Wea. Rev.*, **101**, 44–55.

Kraus, E. B., 1963: The diurnal precipitation change over the sea. *J. Atmos. Sci.*, **20**, 551–556.

Lenschow, D. H., 1973: Two examples of planetary boundary layer modification over the Great Lakes. *J. Atmos. Sci.*, **30**, 568–581.

Lilly, D. K., 1968: Models of cloud-topped mixed layers under a strong inversion. *Quart. J. Roy. Meteor. Soc.*, **94**, 292–309.

Malkus, J. S., 1958: On the structure of the trade wind moist layer. *Papers Phys. Oceanogr. Meteor.*, **13**, No. 2.

Miller, D. B., and R. G. Feddes, 1971: Global atlas of relative cloud cover 1967–1970. Joint production by U. S. Dept. of Commerce and U. S. Air Force, Washington D. C. [Available from NTIS, Springfield, Va., AD739 434].

Neiburger, M., D. S. Johnson and C. W. Chien, 1961: Studies of the structure of the atmosphere over the Eastern Pacific Ocean in summer, I, The inversion over the Eastern North Pacific Ocean *Univ. Calif. Publ. Meteor.*, **1**, No. 1.

Nitta, T., 1975: Observational determination of cloud mass flux distributions. *J. Atmos. Sci.*, **32**, 73–91.

——, and S. Esbensen, 1974: Heat and moisture budget analyses using BOMEX data. *Mon. Wea. Rev.*, **102**, 17–28.

Ooyama, K., 1971: A theory on parameterization of cumulus convection. *J. Meteor. Soc. Japan*, **49**, 744–756.

Riehl, H., T. C. Yeh, J. S. Malkus and N. E. La Seur, 1951: The northeast trade of the Pacific Ocean. *Quart. J. Roy. Meteor. Soc.*, **77**, 598–626.